ACS APPLIED MATERIALS & INTERFACES

Research Article

www.acsami.org

Asymmetrical Squaraines Bearing Fluorine-Substituted Indoline Moieties for High-Performance Solution-Processed Small-Molecule Organic Solar Cells

Daobin Yang,[†,‡] Lin Yang,[†] Yan Huang,*[,†] Yan Jiao,[†] Tsukasa Igarashi,[‡] Yao Chen,[†] Zhiyun Lu,*[,†] Xuemei Pu,[†] Hisahiro Sasabe,*[,‡] and Junji Kido*[,‡]

[†]Key Laboratory of Green Chemistry and Technology (Ministry of Education), College of Chemistry, Sichuan University, Chengdu 610064, People's Republic of China

[‡]Department of Organic Device Engineering, Research Center for Organic Electronics, Yamagata University, Yonezawa 992-8510, Japan

Supporting Information

ABSTRACT: Two novel asymmetrical squaraines based on the indoline unit, ASQ-5-F and ASQ-5-DF, with one and two fluorine substituents, have been developed to investigate the effect of fluorine substituted on small-molecule bulk-heterojunction (BHJ) organic solar cells (OSCs). In comparison with non-fluorine-substituted ASQ-5, both fluorine-substituted ASQ-5-F and ASQ-5-DF possess analogous absorption band gaps but 0.05 and 0.10 eV lowered highest occupied molecular orbital (HOMO) energy levels, respectively. Single-crystal analysis exhibits that ASQ-5-DF shows more desirable intermolecular packing patterns for the hole-carrier collection than ASQ-5 does; hence, higher hole mobility could be acquired. Therefore, solution-processed small-molecule BHJ OSCs fabricated with ASQ-5-F/$PC_{71}BM$ and ASQ-5-DF/$PC_{71}BM$ blends exhibit extremely higher power conversion efficiency (PCE; 5.0% and 6.0%, respectively) than that of ASQ-5/$PC_{71}BM$ (4.5%). The much improved PCE could be attributed to the simultaneously enhanced V_{oc}, J_{sc}, and FF relative to those of the ASQ-5-based device. To our knowledge, this is the highest PCE (6.0%) among squaraine-based solution-processed BHJ OSCs and the highest PCE in OSCs based on the fluorinated donor segment of small molecules.

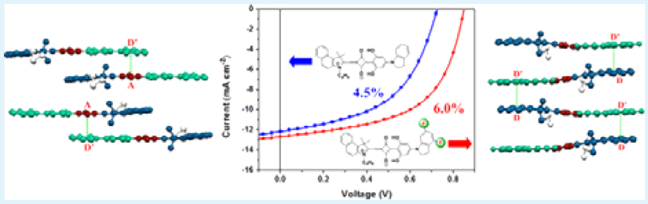

KEYWORDS: *asymmetrical squaraines, fluorine-substituted, packing pattern, solution-processed, small-molecule organic solar cells*

1. INTRODUCTION

Recently, solution-processed bulk-heterojunction (BHJ) organic solar cells (OSCs) using small-molecule compounds as electron-donor materials have attracted increasing research interest owing to their well-defined molecular structure, accurate molecular weight, high purity without batch-to-batch variation, and easy mass-scale production of small molecules relative to their polymeric counterparts.[1−6] Among the hitherto developed small-molecule OSC materials, squaraine (SQ) materials have drawn much attention because of their high molar extinction coefficients, intense and broad absorption in vis−near-IR spectral regions, and good photostability.[7−16] However, despite much research effort in exploiting OSC SQ materials, the record power conversion efficiency (PCE) of solution-processed SQ-based BHJ OSC is just 5.50%.[17] Note that the SQ compound used in this device was a symmetrical squaraine (SSQ) bearing a D−A−D skeleton with the same electron-donating (D) segments and was first used as an OSC material in 2009.[18]

In comparison with SSQs, asymmetrical squaraines (ASQs) bearing D−A−D′ molecular frameworks should afford plenty more room for molecular tailoring,[19,20] yet BHJ OSCs using ASQs as electron donors just show a poor performance (PCE_{max} = 2.05%).[21] Very recently, we have developed a series of novel ASQs with 1,1,2-trimethyl-1*H*-benzo[*e*]indole as the D subunit, 2,6-dihydroxyphenyl bearing different end-capping groups at the 4 postion as the D′ segment, and a squaric acid core as the A segment.[22−25] Encouragingly, one of the compounds, ASQ-5 with an indoline end capper (the structure is shown in Figure 1), was demonstrated to be a high-performance OSC material because the PCE of an ASQ-5-based device could reach 4.29%,[23] which was the record among ASQ-based OSCs. However, the performance of an ASQ-5-based device is still inferior to that of the best device using SSQ as the electron donor,[17] which should be ascribed to the relatively low open-circuit voltage (V_{oc}, 0.81 V) stemming from the relatively high highest occupied molecular orbital (HOMO) energy level of ASQ-5 (−5.09 eV). Hence, we aimed at exploitation of the ASQ-5 derivatives with declined HOMO energy levels, so that V_{oc} was enhanced and, hence, higher PCE could be acquired in the corresponding OSC devices.

Received: April 24, 2015
Accepted: June 1, 2015
Published: June 1, 2015

DOI: 10.1021/acsami.5b03558
ACS Appl. Mater. Interfaces 2015, 7, 13675−13684

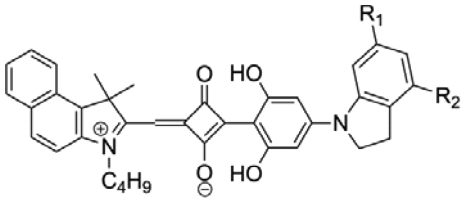

Figure 1. Molecular structures of the reference and objective compounds.

According to literature reports, fluorine substitution is a well-adopted strategy with regard to the decline of HOMO energy levels of OSC electron-donor materials.[26,27] Additionally, the strongly induced dipole in C−F bonds could endow the compounds with intensified intermolecular interactions and, hence, high charge carrier mobility, which would be beneficial to the enhancement of both the short-circuit current density (J_{sc}) and fill factor (FF) of the OSC devices.[28,29] However, most of the current studies were focused on fluorination of the A subunit in D−A-structured copolymers.[30,31] To the best of our knowledge, two literatures could be found using fluorinated D subunits to construct small-molecule OSC electron-donor materials, while in both cases, the fluorine atom was exclusively introduced into the para position on the D moiety.[32,33] Nevertheless, compared with those of the pristine molecules, the HOMO energy levels of the fluorinated compounds were found to be dropped just slightly (0.02 eV), and the PCE of the corresponding BHJ OSC devices were unsatisfactory (1.63% and 3.15%). In fact, although the fluorine atom can usually be considered as a strong electron-withdrawing substituent, according to the report from De Cola et al.,[34] the fluorine atom should show a double nature, i.e., inductive and mesomeric; thus, the meta site of the groups with respect to the fluorination position should be more electron-deficient than the para one. Consequently, ASQ-5-F and ASQ-5-DF bearing molecular skeletons similar to that of ASQ-5, but with one or two fluorine atoms on the meta site(s) of the indoline end-capping group with respect to its nitrogen atom (Figure 1), were designed and synthesized. In comparison with the reference compound ASQ-5, both of the fluorinated objective compounds exhibit analogous absorption band gaps but deeper HOMO energy levels. In addition, more desirable packing patterns for hole-carrier collection could be observed in a single-crystal sample of ASQ-5-DF than those of ASQ-5. As a result, BHJ OSCs based on both ASQ-5-F and ASQ-5-DF show 0.06−0.11 V enhanced V_{oc}; in fact, the ASQ-5-DF device shows an impressive V_{oc} of 0.93 V; increased J_{sc} could also be acquired in the ASQ-5-DF-based device, which is chiefly attributed to the higher hole mobility of the active layer. Therefore, the solution-processed BHJ OSC with ASQ-5-DF as the electron donor exhibits much more enhanced performance than that with the ASQ-5 device, and the maximum PCE is as high as 6.04%, which is even higher than those of the best SSQ-based devices.[17] To our knowledge, this is the highest PCE (6.04%) among solution-processed SQ-based BHJ OSCs and one of the highest PCEs in BHJ OSCs based on fluorinated small-molecule materials.[35−37]

2. EXPERIMENTAL SECTION

2.1. Instruments and Characterization. ^{1}H and ^{13}C NMR spectra were measured using a Bruker Avance AV II 400 MHz spectrometer, and the chemical shifts were recorded in units of ppm with tetramethylsilane as the internal standard. High-resolution mass spectrometry (HR-MS) spectra were obtained from a Shimadzu LCMS-IT-TOF spectrometer. Thermogravimetry analysis (TGA) was performed on a PerkinElmer TGA Q500 instrument in an atmosphere of N_2 at a heating rate of 10 °C min^{-1}. The purity of the target compounds was measured by EZChrom Elite for high-performance liquid chromatography (Hitachi DAD and RI detectors). Single-crystal X-ray diffraction data of ASQ-5-DF were obtained on a Xcalibur E X-ray single-crystal diffractometer equipped with graphite-monochromated Mo Ka (λ = 0.71073 Å) radiation. Data collection was executed using the *CrysAlisPro* program. The structure of ASQ-5-DF was determined using direct methods and successive Fourier difference syntheses (*SHELXS-97*) and refined using a full-matrix least-squares procedure on F^2 with anisotropic thermal parameters for all non-hydrogen atoms (*SHELXL-97*). A single-crystal X-ray structure was obtained from a metallic-lustered yellow single crystal of ASQ-5-DF obtained from the slow vapor diffusion of *n*-hexane into a dichloromethane (DCM) solution (CCDC 1039544). Packing analysis of the crystal cells was carried out using the *Mercury* program. The ground-state geometries and electronic structures of these target molecules were calculated with *Gaussian 09* software, using density functional theory (DFT) based on the B3LYP/6-31G(d) and B3LYP/6-311G(d,p) levels.

The electronic absorption spectra of the reference and objective compounds in both dilute solution and thin solid film states were recorded using a PerkinElmer Lamdba 950 UV−vis scanning spectrophotometer. The solution samples were prepared in a chloroform solution with a concentration of 3.00 × 10^{-6} mol L^{-1}, while the film samples were obtained by spin-coating from the corresponding chloroform solutions (5 mg mL^{-1}, 1400 rpm/30 s) on quartz substrates. Cyclic voltammetry (CV) measurements were carried out in 2.5 × 10^{-4} mol L^{-1} anhydrous DCM with tetrabutylammonium perchlorate under an argon atmosphere at a scan rate of 50 mV s^{-1} using a LK 2005A electrochemical workstation. The CV system was constructed using a platinum disk, a platinum wire, and Ag/$AgNO_3$ (0.1 mol L^{-1} in acetonitrile) as the working, counter, and reference electrodes, respectively, and the potential of the Ag/$AgNO_3$ reference electrode was internally calibrated using the ferrocene/ferrocenium redox couple (Fc/Fc$^+$), which has a known reduction potential of −4.80 eV relative to the vacuum level. The morphologies of the active layers were analyzed through atomic force microscopy (AFM) in tapping mode under ambient conditions using a MFP 3D Asylum Research instrument.

2.2. Fabrication and Characterization of OSCs. Small-molecule BHJ OSCs were fabricated using indium−tin oxide (ITO)-coated glass as the substrate. The sheet resistance of the ITO layer is 15 Ω sq^{-1}. Patterned ITO-coated glass substrates were sequentially cleaned using detergent, deionized water, acetone, and isopropyl alcohol in an ultrasonic bath for 20 min each. The cleaned substrates were dried in an oven at 65 °C for 12 h before use. The substrate was treated by UV ozone for 30 min and then immediately transferred into a high-vacuum chamber for the deposition of 8 nm of MoO_3 at a pressure of less than 1 × 10^{-4} Pa with a rate of 0.2 Å s^{-1}. Subsequently, photoactive layers (thickness: 60 ± 5 nm) were fabricated by spin-coating a blend of the ASQ compounds and $PC_{71}BM$ in chloroform with a total concentration of 20 mg mL^{-1} in a N_2-filled glovebox at 25 °C. Finally, the substrates were transferred back to the high-vacuum chamber, where C_{70} (7 nm), BCP (5 nm), and Al (100 nm) were deposited as the top electrode at a pressure of less than 2 × 10^{-4} Pa with rates of 0.20, 0.20, and 2.0−3.0 Å s^{-1}, respectively, resulting in a final organic photovoltaic (OPV) cell with a structure of ITO/MoO_3 (8 nm)/ASQ:$PC_{71}BM$/C_{70} (7 nm)/BCP (5 nm)/Al (100 nm). The active area of the OPV cells is 9 mm^2. The current density−voltage (J−V) and external quantum efficiency (EQE) characteristics of the solar cells were measured on a CEP-2000 integrated system

DOI: 10.1021/acsami.5b03558
ACS Appl. Mater. Interfaces 2015, 7, 13675−13684

Scheme 1. Synthetic Routes to the Target Compounds[a]

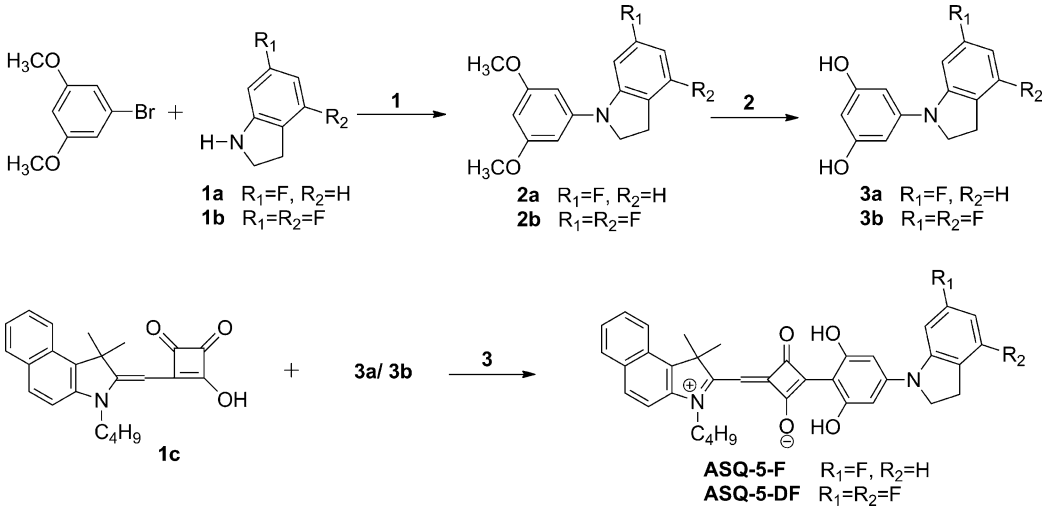

[a](1) NaOBu-*t*, $Pd(OAc)_2$, $P(t\text{-}Bu)_3HBF_4$, toluene, reflux for 8 h; (2) BBr_3, DCM, room temperature, 12 h; (3) *n*-butanol and toluene (1/1), 140 °C, 36 h.

manufactured by Bunkoukeiki Co. Integration of the EQE data over a AM1.5G solar spectrum yielded calculated J_{sc} values with an experimental variation of less than 3% relative to the J_{sc} value measured under 100 mW cm^{-2} simulated AM1.5G light illumination. Hole- and electron-only devices were fabricated with structures of ITO/MoO_3 (8 nm)/ASQ:$PC_{71}BM$ (60 nm)/MoO_3 (8 nm)/Al (100 nm) and ITO/Ca (2 nm)/ASQ:$PC_{71}BM$ (60 nm)/C_{70} (7 nm)/BCP (5 nm)/Al (100 nm), respectively.

2.3. Synthesis. Benzo[*e*]indole semisquarylium (**1c**) and ASQ-5 were prepared according to the procedures described in the literature.[22] *n*-Butanol and toluene were distilled from freshly prepared sodium prior to use. All other chemicals were obtained from commercial sources and used as-received without further purification.

*6-Fluoroindoline (**1a**).* To a solution of 6-fluoroindole (0.54 g, 4.00 mmol) in glacial acetic acid (5 mL) under argon was added in one portion of sodium cyanoborohydride ($NaBH_3CN$; 0.30 g, 4.80 mmol). After the addition, the mixture was stirred for 1 h at room temperature. Then the reaction mixture was poured into an icy 4 M aqueous NaOH solution until a strong basic pH was obtained. The mixture was extracted with ethyl acetate three times. The combined organic phases were washed with a saturated aqueous $NaHCO_3$ solution and water and dried over anhydrous Na_2SO_4, and then the solvents were removed under reduced pressure. The crude product was purified by silica gel chromatography (eluent: hexane/DCM = 1/1) to afford compound **1a** as a colorless liquid (0.23 g, 42%). ^1H NMR (400 MHz, $CDCl_3$): δ 7.00−6.97 (m, 1H, ArH), 6.38−6.31 (m, 2H, ArH), 3.61 (t, 2H, J = 8.4 Hz, NCH_2), 2.99 (t, 2H, J = 8.4 Hz, CH_2).

*4,6-Difluoroindoline (**1b**).* Compound **1b** was obtained as a pale-brown oil (0.52 g, 52%) from the reaction of 4,6-difluoroindole (1.00 g, 6.54 mmol) and $NaBH_3CN$ (2.05 g, 32.7 mmol) following a procedure similar to that described for the synthesis of compound **1a**. ^1H NMR (400 MHz, $CDCl_3$): δ 6.14−6.09 (m, 2H, ArH), 3.66 (t, 2H, J = 8.0 Hz, NCH_2), 3.04 (t, 2H, J = 8.0 Hz, NCH_2).

*N-(3,5-Dimethoxyphenyl)-6-fluoroindoline (**2a**).* A mixture of compound **1a** (0.45 g, 3.28 mmol), 1-bromo-3,5-dimethoxybenzene (0.72 g, 3.32 mmol), sodium *tert*-butoxide (NaOBu-*t*; 0.63 g, 6.56 mmol), palladium(II) acetate [$Pd(OAc)_2$; 22 mg, 3%], and tri-*tert*-butylphosphine tetrafluoroborate] ($P(t\text{-}Bu)_3HBF_4$; 57 mg, 6%) was dissolved in 60 mL of toluene and refluxed under argon for 8 h. The reaction mixture was cooled and passed through filter paper to remove insoluble material, and then the solvents were removed under reduced pressure. The crude product was purified by silica gel chromatography (eluent: hexane/DCM = 5/1) to afford compound **2a** as a pale-yellow oil (0.48 g, 53%). ^1H NMR (400 MHz, $CDCl_3$): δ 7.05 (t, 1H, J = 7.2 Hz, ArH), 6.88 (dd, 1H, J = 10.8 and 2.4 Hz, ArH), 6.44−6.39 (m, 1H, ArH), 6.16 (t, 1H, ^3J = 2.4 Hz, ArH), 4.00 (t, 2H, J = 8.4 Hz, NCH_2), 3.81 (s, 6H, OCH_3), 3.08 (t, 2H, J = 8.4 Hz, CH_2).

*N-(3,5-Dimethoxyphenyl)-4,6-difluoroindoline (**2b**).* Compound **2b** was obtained as a white crystal (0.77 g, 79%) from the reaction of compound **1b** (0.52 g, 3.35 mmol) and 1-bromo-3,5-dimethoxybenzene (0.76 g, 3.52 mmol) according to the procedure described for the synthesis of compound **2a**. Mp: 98−99 °C. ^1H NMR (400 MHz, $CDCl_3$): δ 6.65 (dd, 1H, J = 10.4 and 2.0 Hz, ArH), 6.36 (d, 2H, ^3J = 2.0 Hz, ArH), 6.22−6.16 (m, 2H, ArH), 4.03 (t, 2H, J = 8.4 Hz, NCH_2), 3.81 (s, 6H, OCH_3), 3.11 (t, 2H, J = 8.4 Hz, CH_2).

*5-(6-Fluoroindolin-1-yl)benzene-1,3-diol (**3a**).* Compound **2a** (0.45 g, 1.64 mmol) was added to 50 mL of anhydrous CH_2Cl_2, boron tribromide (10 mL of a 1 M solution in CH_2Cl_2, 9.85 mmol) was added dropwise slowly under an ice bath, and then the solution was stirred at room temperature for 12 h. The solution was then decanted to 150 mL of icy water to remove any excess of BBr_3. The organic phase was separated, and the aqueous phase was extracted with CH_2Cl_2 three times. The combined organic phases were washed with a saturated aqueous $NaHCO_3$ solution and water and dried over anhydrous Na_2SO_4, and then the solvents were removed under reduced pressure. The crude product was purified by silica gel chromatography (eluent: DCM/methanol = 50/1) to afford compound **3a** as a pale-yellow viscous liquid (0.40 g, 89%).

*5-(4,6-Difluoroindolin-1-yl)benzene-1,3-diol (**3b**).* Compound **3b** was obtained as a pale-yellow viscous liquid (0.50 g, 74%) from the reaction of **2b** (0.75 g, 2.57 mmol) and boron tribromide (15 mL of a 1 M solution in CH_2Cl_2, 15.42 mmol) according to the procedure described for the synthesis of **3a**.

4-[(3-Butyl-1,1-dimethyl-1H-benzo[e]indol-3-ium-2-yl)-methylene]-2-[4-(6-fluoroindolin-1-yl)-2,6-dihydroxyphenyl]-3-oxo-cyclobut-1-enolate (ASQ-5-F). A mixture of compounds **1c** (527 mg, 1.46 mmol) and **3a** (400 mg, 1.63 mmol) in *n*-butanol (40 mL) and toluene (40 mL) were added into a round-bottomed flask. The mixture was refluxed with a Dean−Stark apparatus for 36 h. After the mixture was cooled, the solvents were removed under reduced pressure to afford the crude product, which was further purified by silica gel chromatography using 50/1 DCM/methanol (v/v) as the eluent. The resulting green solid was recrystallized from a mixture of DCM and methanol (1/8, v/v) to afford green crystals (600 mg, 70%). Mp: 259−260 °C. ^1H NMR (400 MHz, $CDCl_3$): δ 12.35 (s, 2H, OH), 8.24 (d, 1H, J = 8.4 Hz, ArH), 7.97 (d, 2H, J = 8.4 Hz, ArH), 7.67 (t, 1H, J = 8.0 Hz, ArH), 7.54 (t, 1H, J = 7.2 Hz, ArH), 7.41 (d, 1H, J = 8.8 Hz, ArH), 7.14−7.07 (m, 2H, ArH), 6.59 (t, 1H, J = 8.4 and 2.6 Hz, ArH), 6.25 (s, 2H, ArH), 6.03 (s, 1H, CH), 4.27 (t, 2H, J = 7.6 Hz, NCH_2), 4.10 (t, 2H, J = 8.0 Hz, NCH_2), 3.11 (t, 2H, J = 8.0 Hz,

DOI: 10.1021/acsami.5b03558
ACS Appl. Mater. Interfaces 2015, 7, 13675−13684

CH_2), 2.04 (s, 6H, CH_3), 1.93−1.85 (m, 2H, CH_2), 1.56−1.47 (m, 2H, CH_2), 1.05 (t, 3H, J = 7.2 Hz, CH_3). ^{13}C NMR (100 MHz, $CDCl_3$): δ 176.2, 170.8, 169.0, 163.8, 163.0, 162.0, 161.4, 151.7, 145.7, 145.6, 138.5, 136.4, 132.2, 130.4, 129.8, 128.2, 128.1, 128.1, 127.9, 125.7, 125.5, 125.4, 122.8, 110.5, 107.6, 107.3, 104.6, 100.8, 100.6, 96.6, 88.0, 52.8, 52.4, 44.7, 29.9, 26.4, 20.3, 13.8. HR-MS (ESI). Calcd for $C_{37}H_{34}FN_2O_4$ ([M + H]$^+$): m/z 589.2503. Found: m/z 589.2508. Purity: 99.0% (HPLC; eluent, tetrahydrofuran/water = 6/4).

4-[(3-Butyl-1,1-dimethyl-1H-benzo[e]indol-3-ium-2-yl)-methylene]-2-[4-(4,6-difluoroindolin-1-yl)-2,6-dihydroxyphenyl]-3-oxocyclobut-1-enolate (ASQ-5-DF). ASQ-5-DF was synthesized following a procedure similar to that for the synthesis of ASQ-5-F using compounds **1c** (613 mg, 1.70 mmol) and **3b** (500 mg, 1.89 mmol) as the reactants. The resulting green solid was recrystallized from a mixture of DCM and methanol (1/8, v/v) to afford green crystals (670 mg, 65%). Mp: 262−263 °C. ^{1}H NMR (400 MHz, $CDCl_3$): δ 12.31 (s, 2H, OH), 8.24 (d, 1H, J = 8.4 Hz, ArH), 7.98 (d, 2H, J = 8.8 Hz, ArH), 7.68 (t, 1H, J = 8.0 Hz, ArH), 7.56 (t, 1H, J = 7.6 Hz, ArH), 7.42 (d, 1H, J = 8.8 Hz, ArH), 6.93 (dd, 1H, J = 10 and 2.0 Hz, ArH), 6.35 (t, 1H, J = 8.8 and 2.0 Hz, ArH), 6.23 (s, 2H, ArH), 6.06 (s, 1H, CH), 4.29 (t, 2H, J = 7.2 Hz, NCH_2), 4.12 (t, 2H, J = 8.4 Hz, NCH_2), 3.13 (t, 2H, J = 8.4 Hz, CH_2), 2.04 (s, 6H, CH_3), 1.94−1.86 (m, 2H, CH_2), 1.57−1.47 (m, 2H, CH_2), 1.05 (t, 3H, J = 7.2 Hz, CH_3). ^{13}C NMR (100 MHz, $CDCl_3$): δ 184.0, 180.8, 176.7, 171.5, 168.5, 164.4, 164.3, 162.8, 162.3, 162.0, 161.9, 160.1, 160.0, 157.7, 157.5, 151.1, 147.4, 147.3, 147.3, 147.2, 138.4, 136.6, 132.3, 130.4, 129.9, 128.2, 128.0, 125.9, 122.8, 113.9, 113.8, 113.6, 113.6, 110.6, 104.7, 97.1, 96.9, 96.7, 96.7, 96.4, 96.4, 96.3, 96.1, 95.8, 88.3, 52.8, 52.6, 44.8, 29.9, 26.3, 23.5, 20.3, 13.8. HR-MS (ESI). Calcd for $C_{37}H_{33}F_2N_2O_4$ ([M + H]$^+$): m/z 607.2408. Found: m/z 607.2403. Purity: 99.5% (HPLC; eluent, tetrahydrofuran/water = 6/4).

3. RESULTS AND DISCUSSION

3.1. Synthesis and Characterization. The synthetic routes to the target molecules are illustrated in Scheme 1. ASQ-5-F and ASQ-5-DF were prepared through condensation reactions with **1c** and fluorinated indoline compounds **3a** and **3b** as the reactants with satisfactory yields of ∼65%. Both of them show sufficient solubility (>20 mg mL^{-1}) in common organic solvents like chloroform, chlorobenzene, and 1,2-dichlorobenzene; in addition, high-quality films of ASQ-5-F and ASQ-5-DF could be obtained through spin-coating from solutions, indicating that they are very suitable for solution processing. As shown in Figure 2, in comparison with the reference compound ASQ-5, both of the fluorine-substituted compounds display higher decomposition temperature (Table 1), suggesting that the thermal stability of SQ materials could be improved through fluorine modification.

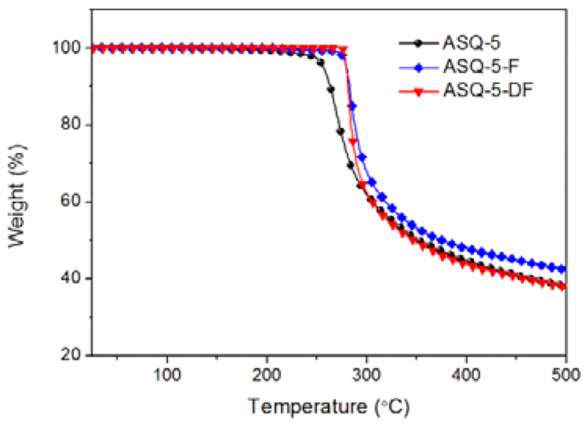

Figure 2. TGA curves of ASQ-5, ASQ-5-F, and ASQ-5-DF.

3.2. Optical Properties. The UV−vis absorption spectra of the objective and reference compounds in chloroform (3.00 × 10^{-6} mol L^{-1}) and thin solid film states are shown in Figure 3, and the data are summarized in Table 1. Similar to ASQ-5, the two fluorine-substituted compounds also show intense absorption at 550−700 nm in dilute solution, with a considerably high molar extinction coefficient of >10^5. In both dilute solution and thin solid film states, the absorption maximum of ASQ-5-F is blue-shifted by 7 nm from that of ASQ-5, while that of ASQ-5-DF is blue-shifted by 14 nm. Because the meta-substituted fluorine atom(s) would show a strong electron-withdrawing inductive effect with respect to the nitrogen atom of the indoline segment, the electron density of the nitrogen atom will be decreased to some extent; hence, the resulting ASQ compounds will show slightly shortened conjugation systems relative to ASQ-5 because of the weaker electron-donating capability of the fluorinated indoline relative to the indoline subunits. In both dilute solution and thin solid film states, the absorption bands of all three compounds show comparable full width at half-maximum (fwhm). Determined by the onset position of the absorption spectra of these compounds, the optical band gaps of ASQ-5-F and ASQ-5-DF are calculated as 1.45 and 1.47 eV, respectively, which are 0.02 and 0.04 eV higher than that of ASQ-5. All of these photophysical results indicated that meta fluorination on the indoline D′ subunit with respect to its nitrogen atom would result in compounds with just slightly blue-shifted absorption bands and slightly widened optical band gaps.

3.3. Electrochemistry Properties. To estimate the energy levels of ASQ-5-F and ASQ-5-DF, their electrochemical properties were investigated by CV. As shown in Figure 4 and Table 1, during anodic scanning, quasi-reversible oxidation processes could be observed in both of the objective compounds, and their E_{ox}^{onset} values were determined to be 0.34 and 0.39 V relative to Fc/Fc$^+$ for ASQ-5-F and ASQ-5-DF, respectively. Hence, by comparison with the Fc/Fc$^+$ redox couple whose energy level was −4.80 eV in vacuum, the HOMO energy levels of ASQ-5-F and ASQ-5-DF were calculated as −5.14 and −5.19 eV, respectively, which were 0.05 and 0.10 eV lower than that of ASQ-5 (−5.09 eV). Consequently, meta fluorination on the indoline segment with respect to its nitrogen atom would indeed endow the ASQ-5 derivatives with declined HOMO energy levels, which should be propitious to the enhancement of V_{oc} in their corresponding OSC devices.[38] According to the HOMO energy levels and optical band gaps, the LUMO energy levels of ASQ-5-F and ASQ-5-DF were calculated as −3.69 and −3.72 eV, respectively.[23] In addition, the electron density distributions of the HOMO and LUMO of these compounds are shown in Figure S1 in the Supporting Information (SI), and DFT calculation shows that the HOMO energy levels of ASQ-5, ASQ-5-F, and ASQ-5-DF are −5.17, −5.22, and −5.28 eV, respectively, which are consistent with their corresponding experimental values (−5.09, −5.14, and −5.19 eV, respectively), indicating that these experimental results are reliable.

3.4. Single-Crystal Analysis. To gain insight into the effects caused by fluorination on the intermolecular packing properties of the objective compounds, a single-crystal sample of ASQ-5-DF was prepared. As shown in Figure 5, in ASQ-5-DF, its squarate core and dihydroxyphenyl moiety comprise a quasi-coplanar (dihedral angle <2.5°) geometry due to the strong hydrogen-bonding (O···H−O) interactions between the hydroxy groups on the phenyl segment and the carbonyl groups

DOI: 10.1021/acsami.5b03558
ACS Appl. Mater. Interfaces 2015, 7, 13675−13684

Table 1. Optical and Electrochemical Properties of the ASQ Compounds

	absorption $\lambda_{abs\ max}$ (nm)		fwhm (nm)						
compd	solution ($\varepsilon \times 10^5$)	film	solution	film	E_g^{opt} [eV]	E_{ox}^{onset} [V]	HOMO [eV]	LUMO[a] [eV]	T_d [°C]
ASQ-5	677 (2.29)	718, 656	39	172	1.43	0.29	−5.09	−3.66	256
ASQ-5-F	670 (2.47)	711, 647	38	175	1.45	0.34	−5.14	−3.69	280
ASQ-5-DF	663 (2.20)	704, 640	39	170	1.47	0.39	−5.19	−3.72	280

[a]LUMO = E_g^{opt} + HOMO.

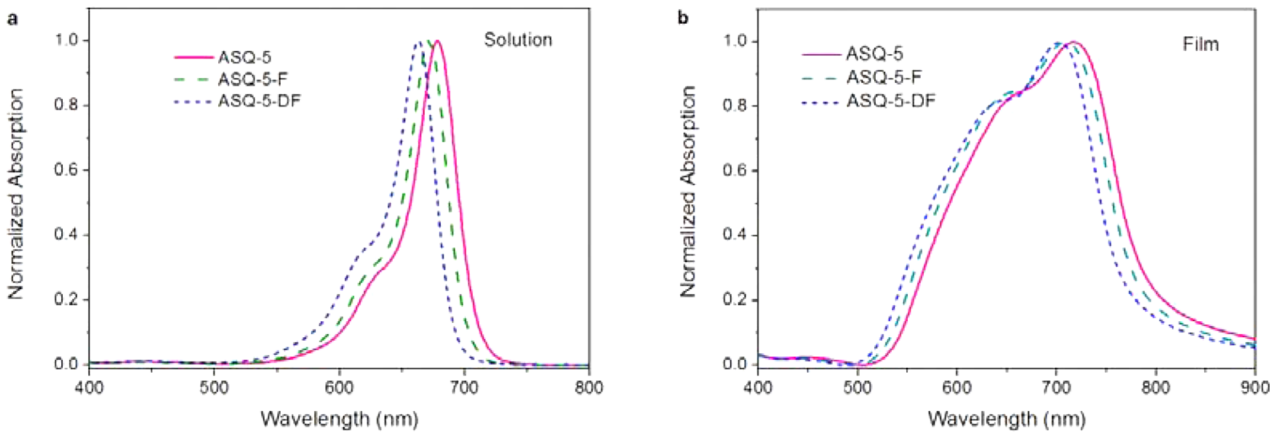

Figure 3. Absorption spectra of the ASQ compounds in (a) solution and (b) thin films.

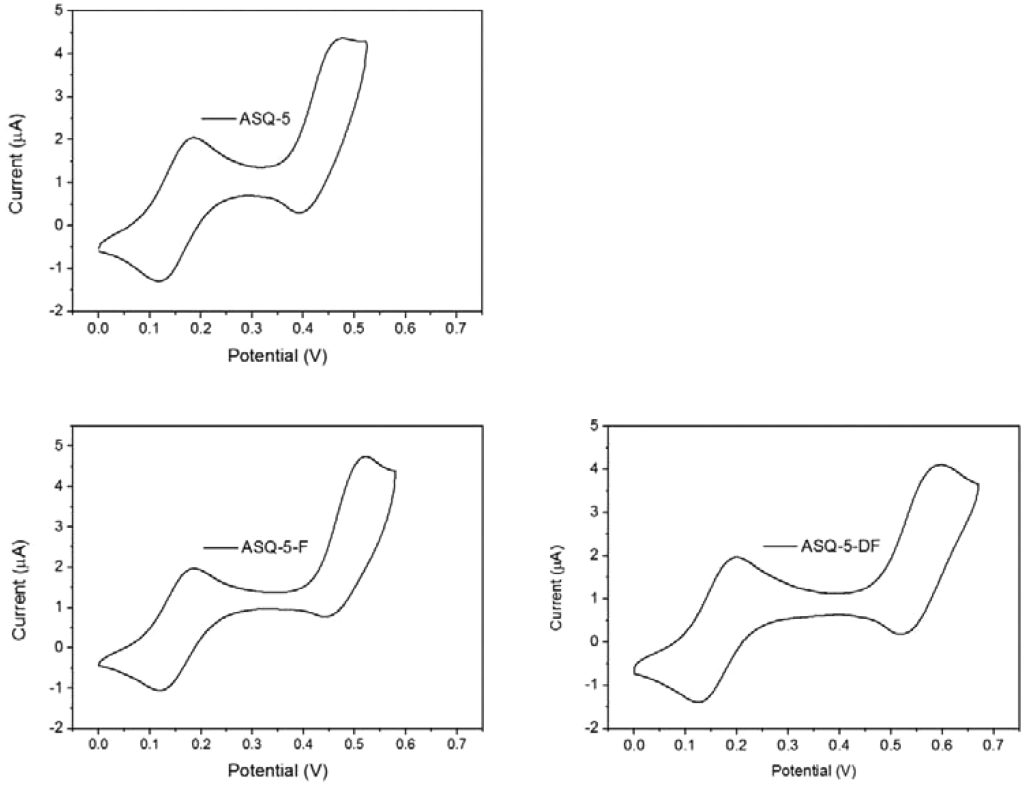

Figure 4. Cyclic voltammograms of ASQ-5, ASQ-5-F, and ASQ-5-DF.

of the squaric acid core. Additionally, in ASQ-5-DF, the lengths of the C−N bond connecting the indoline and phenyl segments (1.39 Å) and the C−C bond linking the squarate core and the phenyl segment (1.42 Å) are both longer than the corresponding bonds of ASQ-5 (1.38 and 1.41 Å, respectively). The elongated C−N and C−C bonds in ASQ-5-DF should be ascribed to its fluorinated indoline subunit with slightly weakened electron-donating capability.

Further investigations on the packing patterns within the crystal structures of ASQ-5-DF and ASQ-5 revealed that both of the compounds show closely packed crystal structures because of the strong face-to-face $\pi-\pi$ intermolecular interactions. More importantly, two distinct packing motifs

DOI: 10.1021/acsami.5b03558
ACS Appl. Mater. Interfaces 2015, 7, 13675−13684

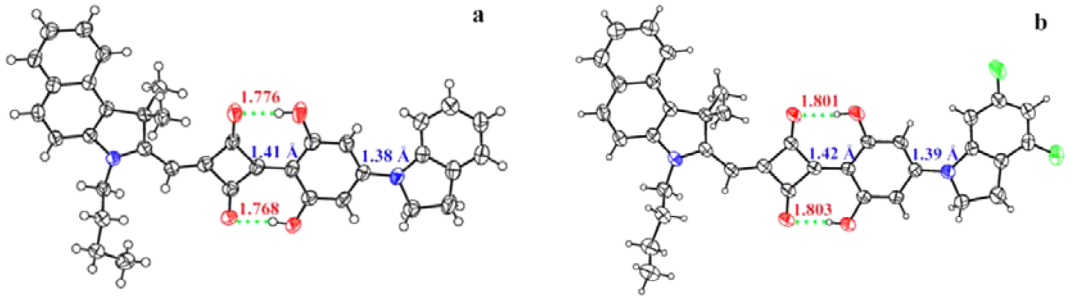

Figure 5. ORTEP diagrams of ASQ-5 (a) and ASQ-5-DF (b).

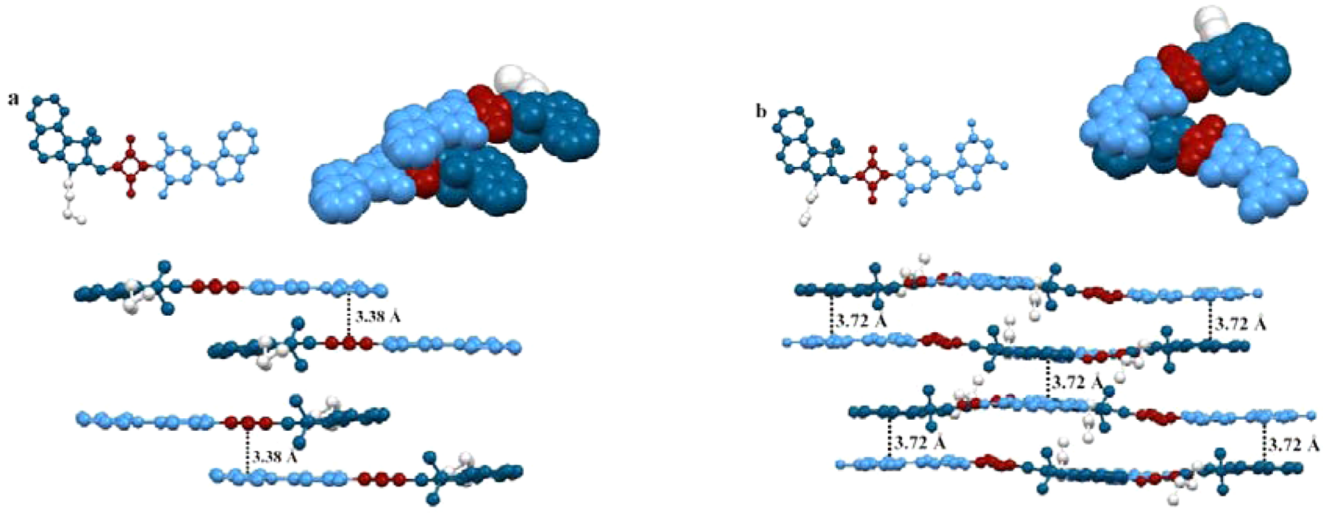

Figure 6. ORTEP diagrams and crystal packings of (a) ASQ-5 and (b) ASQ-5-DF with the A part of the molecule colored red-brown, the D subunit colored deep blue-green, the D′ subunit colored light blue, and the alkyl group on the donor colored light gray. The molecular structure with packing of the respective closest dimers as well as side views is shown to reveal the corresponding $\pi-\pi$-stacking distances of the molecules to their closest neighbors.

Table 2. Photovoltaic Performances of OSCs Based on ASQs: $PC_{71}BM$

donor		V_{oc} [V]	J_{sc} [mA cm^{-2}]	FF	PCE [%][c]	μ_h [cm^2 V^{-1} s^{-1}]	μ_e [cm^2 V^{-1} s^{-1}]
ASQ-5	as-cast	0.82	10.18	0.45	3.76 (3.64)	1.30×10^{-5}	1.40×10^{-4}
	annealed[a]	0.81	10.98	0.45	4.00 (3.84)	1.96×10^{-5}	1.38×10^{-4}
	under thermal testing[b]	0.73	12.16	0.51	4.53 (4.40)	5.86×10^{-5}	1.58×10^{-4}
ASQ-5-F	as-cast	0.88	10.52	0.46	4.26 (4.18)	2.00×10^{-5}	1.52×10^{-4}
	annealed[a]	0.87	11.18	0.46	4.47 (4.34)	2.90×10^{-5}	1.89×10^{-4}
	under thermal testing[b]	0.81	11.99	0.52	5.05 (4.94)	8.62×10^{-5}	2.20×10^{-4}
ASQ-5-DF	as-cast	0.93	11.01	0.46	4.71 (4.60)	2.43×10^{-5}	1.77×10^{-4}
	annealed[a]	0.92	11.56	0.47	5.00 (4.87)	3.40×10^{-5}	2.18×10^{-4}
	under thermal testing[b]	0.85	12.68	0.56	6.04 (5.91)	1.12×10^{-4}	2.69×10^{-4}

[a]The active layers were thermally annealed at 80 °C for 10 min. [b]The devices were tested under 80 °C. [c]The first data are the best PCEs obtained, while those in parentheses are the average values of 12 individual devices.

could be distinguished in ASQ-5 and ASQ-5-DF. As shown in Figure 6, for ASQ-5, although one next-neighboring molecule is located at a quite close interplanar distance of 3.38 Å, its electron-donating indoline segment lies on top of the neighbor's electron-deficient squarate core (A subunit and D−A packing pattern), whereas for ASQ-5-DF, despite the fact that the interplanar $\pi-\pi$-distance is 3.72 Å, extensive $\pi-\pi$ stacking occurs between the benzo[*e*]indole (D subunit) and the electron-donating indoline-modified phenyl groups (D′ subunit and D−D′ packing pattern) of ASQ-5-DF, so that more efficient hole collection would occur.[39] Therefore, upon fluorination, the resulting ASQ derivatives may show better hole mobility because of their more desirable orientation patterns in the condensed state.

3.5. Hole Mobility. The hole mobility of a neat film of the ASQ was evaluated by the space-charge-limited-current method, the hole-only device structure is ITO/MoO_3 (80 Å)/ASQ (600 Å)/Al (1000 Å), and the *J*−*V* characteristics of the devices are shown in Figure S2 in the SI. The hole mobility of the two-fluorine-substituted ASQ-5-DF film was calculated as 9.62×10^{-5} cm^2 V^{-1} s^{-1}, 1.4 times higher than that of the one-fluorine-substituted ASQ-5-F film (6.80×10^{-5} cm^2 V^{-1} s^{-1}) and nearly 2 times higher than that of the reference compound ASQ-5 (4.81×10^{-5} cm^2 V^{-1} s^{-1}). The much increased hole

DOI: 10.1021/acsami.5b03558
ACS Appl. Mater. Interfaces 2015, 7, 13675−13684

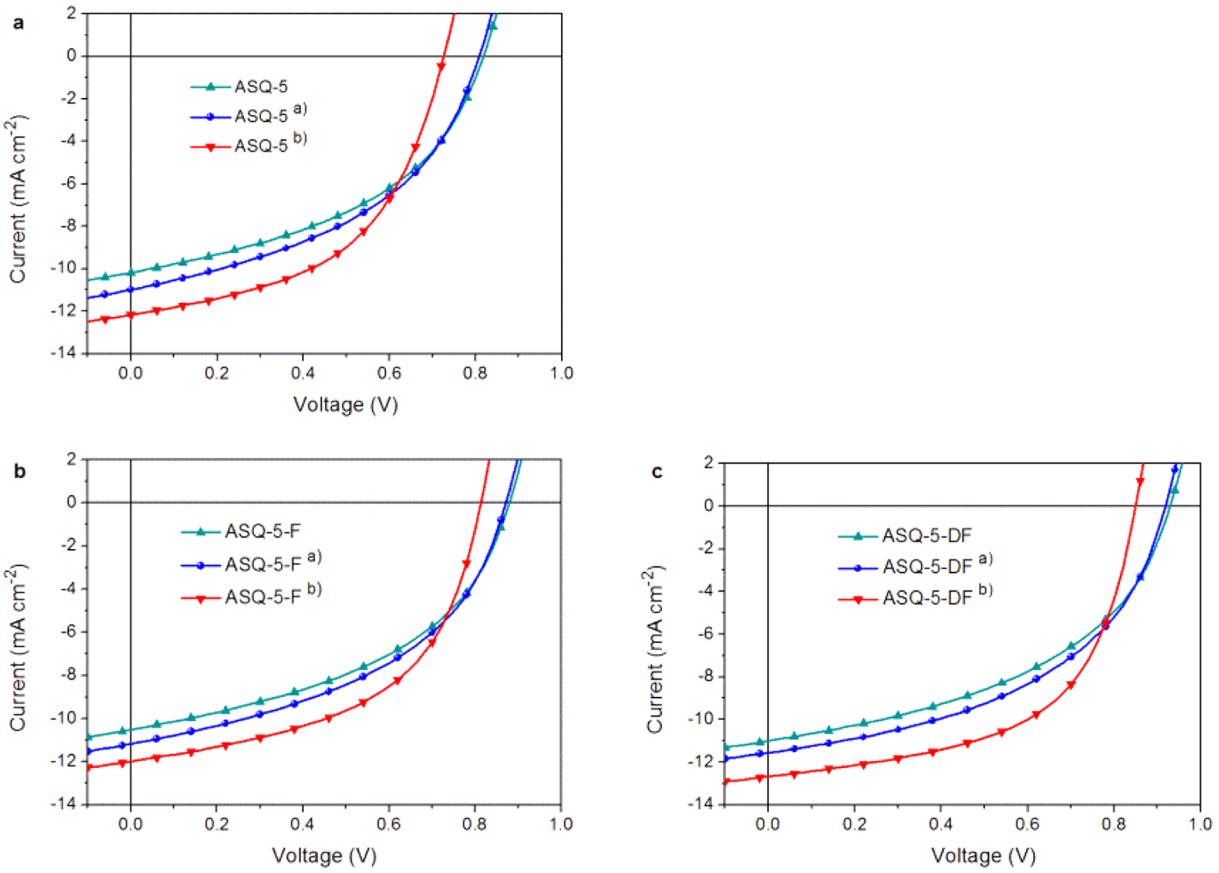

Figure 7. *J*–*V* curve characteristics of ASQ-5-based (a), ASQ-5-F-based (b), and ASQ-5-DF-based (c) OSCs. Footnote a: Thermally annealed devices (80 °C, 10 min). Footnote b: Thermally tested devices (at 80 °C).

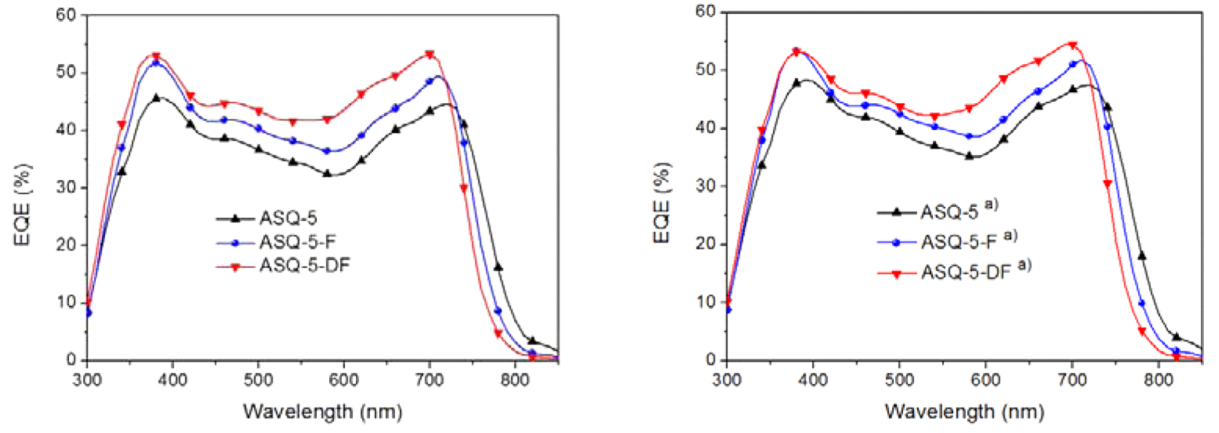

Figure 8. EQE curves of OSCs using ASQ-5, ASQ-5-F, and ASQ-5-DF as electron-donor materials. Footnote a: Devices after having been thermally annealed at 80 °C for 10 min.

mobility of ASQ-5-DF-based samples can most likely be ascribed to its more desirable intermolecular packing patterns.[39]

3.6. OSCs. To evaluate the photovoltaic performance of the objective molecules, BHJ devices with structures of ITO/MoO_3 (8 nm)/ASQ:$PC_{71}BM$ (1/3 in wt %, 60 nm)/C_{70} (7 nm)/BCP (5 nm)/Al (100 nm) were fabricated, where a thin layer (7 nm) of C_{70} was inserted between the active and BCP layers to block the leakage current.[17,40] The photovoltaic properties of these devices are summarized in Table 2, their corresponding current density–voltage (*J*–*V*) curves are illustrated in Figure 7, and their EQE spectra are shown in Figure 8. The ASQ-5-based reference device shows PCE of 3.76%, V_{oc} of 0.82 V, J_{sc} of 10.18 mA cm^{-2}, and FF of 0.45, and the PCE, V_{oc}, J_{sc}, and FF of the ASQ-5-F-based one are 4.26%, 0.88 V, 10.52 mA cm^{-2}, and 0.46, respectively, while those of the ASQ-5-DF-based device are 4.71%, 0.93 V, 11.01 mA cm^{-2}, and 0.46, respectively. In comparison with the reference device, the ASQ-5-F-based device shows 0.06 V higher V_{oc}, while the ASQ-5-DF-based device exhibits 0.11 V higher V_{oc}. These observations are consistent with the electrochemical measurements of the HOMO energy levels of ASQ-5-F and ASQ-5-DF as 0.05 and 0.10 eV lower than that of ASQ-5. In addition to its much enhanced V_{oc}, the ASQ-5-DF-based device shows a more enhanced J_{sc} than that of the reference device, despite the fact

DOI: 10.1021/acsami.5b03558
ACS Appl. Mater. Interfaces 2015, 7, 13675–13684

that ASQ-5-DF shows a 14 nm blue-shifted absorption band relative to ASQ-5 in the thin film state. In principle, J_{sc} correlates highly with the light-harvesting capability, carrier mobility, and morphology of the active layer.[41−43] To elucidate the origin of the enhanced J_{sc} in the ASQ-5-DF device, the EQE curves of the three as-prepared devices were recorded. As shown in Figure 8, in comparison with the reference device, the ASQ-5-DF device shows a narrower spectral response to EQE, yet its EQE values in 400−700 nm are much higher; hence, the increased J_{sc} in the ASQ-5-DF device should not be attributed to the enhanced light-harvesting capability of ASQ-5-DF relative to ASQ-5. Subsequent AFM characterization results revealed that the ASQ-5/$PC_{71}BM$, ASQ-5-F/$PC_{71}BM$, and ASQ-5-DF/$PC_{71}BM$ composite films show quite smooth surfaces with an analogous root-mean-square (rms) of ∼0.56 nm, respectively (Figures S3−S5 in the SI). Therefore, the increased J_{sc} of the ASQ-5-DF device may originate from the higher hole mobility (μ_h) of its active layer. Accordingly, the μ_h values of the ASQ-5/$PC_{71}BM$ and ASQ-5-DF/$PC_{71}BM$ blending films (1/3) were measured, and the data are summarized in Table 2 and the $J-V$ characteristics in Figure S6 in the SI. As expected, the ASQ-5-DF/$PC_{71}BM$ composite film shows nearly 1 times higher μ_h than that of the ASQ-5/$PC_{71}BM$ blending film (2.43×10^{-5} cm^2 V^{-1} s^{-1} vs 1.30×10^{-5} cm^2 V^{-1} s^{-1}), which could be attributed to the more desirable packing patterns in ASQ-5-DF than in ASQ-5 for the hole-carrier collection according to single-crystal structure analysis. Additionally, the increased J_{sc} value of the ASQ-5-F device is also attributed to the higher μ_h of its active layer than that of ASQ-5 (shown in Table 2).

Upon thermal annealing (80 °C, 10 min), all three devices show enhanced performance, which could be attributed to the increased μ_h and better balanced hole and electron mobilities in the active layers (Table 2) and morphology (Figures S3−S5 in the SI). Similar to those of as-prepared devices, the highest PCE of 5.00% and 4.47% could be achieved in ASQ-5-DF- and ASQ-5-F-based devices, respectively, while the lowest PCE of 4.00% could be obtained in the reference device. Taking into consideration that the outdoor working temperature of the solar cells is generally higher than that under ambient conditions, these OSC devices were tested under 80 °C.[44] Excitingly, for all three devices, although their V_{oc} values were found to drop slightly,[45] both of their J_{sc} and FF values were observed to be enhanced significantly under thermal testing (Table 2), resulting in much higher PCE values. It is worth noting that, under thermal testing, the PCE of the ASQ-5-DF-based device could be enhanced by ∼20% compared to that of the thermally annealed one and could reach as high as 6.04%. In-depth carrier-mobility measurements revealed that when the measurements were carried out at 80 °C, the μ_h values of all of the active layers were drastically increased (e.g., the μ_h value of ASQ-5-DF/$PC_{71}BM$ increased 2.3 times), while the electron mobility (μ_e) of the active layer just increased slightly (e.g., the μ_e value of ASQ-5-DF/$PC_{71}BM$ increased 0.2 times and the corresponding $J-V$ characteristics are given in Figure S7 in the SI). As a result, for the ASQ-5-DF-based devices, the μ_e/μ_h ratio could be dropped from 6.4 to 2.4 before and after thermal testing. Thereupon, in the thermally tested ASQ-5-DF-based device, the much enhanced μ_h, together with considerably balanced hole and electron mobility of the active layer, would result in a much higher charge-carrier extraction efficiency, which should account for its high performance.[45] After being cooled to room temperature, all of these devices just showed OSC performances similar to those of the annealed ones, which is very promising for practical applications.

4. CONCLUSION

In conclusion, by meta fluorination on the indoline electron-donating end-capping group of ASQ-5, two novel ASQ materials, ASQ-5-F and ASQ-5-DF, showing comparable absorption characteristics but more declined HOMO energy levels were developed. In comparison with ASQ-5, the difluorinated ASQ-5-DF not only possesses a 0.11 V lowered HOMO energy level but also shows more desirable intermolecular packing patterns for hole-carrier collection; hence, higher hole mobility could be acquired in the active layer of its OSCs. Consequently, the solution-processed ASQ-5-DF-based BHJ OSC shows both higher V_{oc} and J_{sc} than those of the ASQ-5-based reference device, and a high PCE of 6.04% could be achieved, which is the record one among the hitherto-reported solution-processed SQ-based BHJ OSCs, and the highest PCE in BHJ OSC based on the fluorinated donor segment of small molecules. Our results show the importance of molecular tailoring for achieving high-performance OSC materials, and meta fluorination on the D subunits may shed light on the molecular design strategy for D−A-structured electron-donor materials to achieve high PCE.

■ ASSOCIATED CONTENT

Supporting Information

X-ray crystallographic data in CIF format, crystal data, electron density distribution, $J-V$ curves, AFM 3D images and charge-carrier-mobility calculation. This Supporting Information is available free of charge via the Internet at The Supporting Information is available free of charge on the ACS Publications website at DOI: 10.1021/acsami.5b03558.

■ AUTHOR INFORMATION

Corresponding Authors

*E-mail: huangyan@scu.edu.cn (Y.H.).
*E-mail: luzhiyun@scu.edu.cn (Z.L.).
*E-mail: h-sasabe@yz.yamagata-u.ac.jp (H.S.).
*E-mail: kid@yz.yamagata-u.ac.jp (J.K.).

Notes

The authors declare no competing financial interest.

■ ACKNOWLEDGMENTS

We acknowledge financial support for this work by the National Natural Science Foundation of China (Projects 21190031, 21372168, and 21432005) and China Scholarship Council. We are grateful to the Analytical & Testing Center of Sichuan University and Comprehensive Training Platform of Specialized Laboratory, College of Chemistry, Sichuan University, for providing NMR, HR-MS, and single-crystal X-ray diffraction data for the intermediates and objective molecules.

■ REFERENCES

(1) Gupta, V.; Kyaw, A. K. K.; Wang, D. H.; Chand, S.; Bazan, G. C.; Heeger, A. J. Barium: An Efficient Cathode Layer for Bulk-heterojunction Solar Cells. *Sci. Rep.* **2013**, *3*, 1965.

(2) Zhang, Q.; Kan, B.; Liu, F.; Long, G.; Wan, X.; Chen, X.; Zuo, Y.; Ni, W.; Zhang, H.; Li, M.; Hu, Z.; Huang, F.; Cao, Y.; Liang, Z.; Zhang, M.; Russell, T. P.; Chen, Y. Small-Molecule Solar Cells with Efficiency over 9%. *Nat. Photonics* **2015**, *9*, 35−41.

(3) Kan, B.; Zhang, Q.; Li, M.; Wan, X.; Ni, W.; Long, G.; Wang, Y.; Yang, X.; Feng, H.; Chen, Y. Solution-Processed Organic Solar Cells

DOI: 10.1021/acsami.5b03558
ACS Appl. Mater. Interfaces 2015, 7, 13675−13684

Based on Dialkylthiol-Substituted Benzodithiophene Unit with Efficiency near 10%. *J. Am. Chem. Soc.* **2014**, *136*, 15529−15532.
(4) Lin, Y.; Li, Y.; Zhan, X. Small Molecule Semiconductors for High-Efficiency Organic Photovoltaics. *Chem. Soc. Rev.* **2012**, *41*, 4245−4272.
(5) Mishra, A.; Bauerle, P. Small Molecule Organic Semiconductors on the Move: Promises for Future Solar Energy Technology. *Angew. Chem., Int. Ed.* **2012**, *51*, 2020−2067.
(6) Zhang, L.; Colella, N. S.; Cherniawski, B. P.; Mannsfeld, S. C. B.; Briseno, A. L. Oligothiophene Semiconductors: Synthesis, Characterization, and Applications for Organic Devices. *ACS Appl. Mater. Interfaces* **2014**, *6*, 5327−5343.
(7) Mayerhoffer, U.; Deing, K.; Gru *β*, K.; Braunschweig, H.; Meerholz, K.; Wurthner, F. Outstanding Short-Circuit Currents in BHJ Solar Cells Based on NIR-Absorbing Acceptor-Substituted Squaraines. *Angew. Chem., Int. Ed.* **2009**, *48*, 8776−8779.
(8) Bagnis, D.; Beverina, L.; Huang, H.; Silvestri, F.; Yao, Y.; Yan, H.; Pagani, G. A.; Marks, T. J.; Facchetti, A. Marked Alkyl- vs Alkenyl-Substitutent Effects on Squaraine Dye Solid- State Structure, Carrier Mobility, and Bulk-Heterojunction Solar Cell Efficiency. *J. Am. Chem. Soc.* **2010**, *132*, 4074−4075.
(9) Wei, G.; Xiao, X.; Wang, S.; Zimmerman, J. D.; Sun, K.; Diew, V. V.; Tompson, M. E.; Forrest, S. R. Arylamine-Based Squaraine Donors for Use in Organic Solar Cells. *Nano Lett.* **2011**, *11*, 4261−4264.
(10) Chen, G.; Sasabe, H.; Wang, Z.; Wang, X.-F.; Hong, Z.; Yang, Y.; Kido, J. Co-Evaporated Bulk Heterojunction Solar Cells with >6.0% Efficiency. *Adv. Mater.* **2012**, *24*, 2768−2773.
(11) Lam, S. L.; Liu, X.; Zhao, F.; Lee, C-L. K.; Kwan, W. L. Manipulating Open-Circuit Voltage in an Organic Photovoltaic Device via a Phenylalkyl Side Chain. *Chem. Commun.* **2013**, *49*, 4543−4545.
(12) Huang, J.-S.; Goh, T.; Li, X.; Sfeir, M. Y.; Bielinski, E. A.; Tomasulo, S.; Lee, M. L.; Hazari, N.; Taylor, A. D. Polymer Bulk Heterojunction Solar Cells Employing Förster Resonance Energy Transfer. *Nat. Photonics* **2013**, *7*, 479−485.
(13) Chen, G.; Sasabe, H.; Sasaki, Y.; Katagiri, H.; Wang, X.-F.; Sano, T.; Hong, Z.; Yang, Y.; Kido, J. A Series of Squaraine Dyes: Effects of Side Chain and the Number of Hydroxyl Groups on Material Properties and Photovoltaic Performance. *Chem. Mater.* **2014**, *26*, 1356−1364.
(14) An, Q.; Zhang, F.; Li, L.; Wang, J.; Zhang, J.; Zhou, L.; Tang, W. Improved Efficiency of Bulk Heterojunction Polymer Solar Cells by Doping Low-Bandgap Small Molecules. *ACS Appl. Mater. Interfaces* **2014**, *6*, 6537−6544.
(15) Sasabe, H.; Igrashi, T.; Sasaki, Y.; Chen, G.; Hong, Z.; Kido, J. Soluble Squaraine Derivatives for 4.9% Efficient Organic Photovoltaic Cells. *RSC Adv.* **2014**, *4*, 42804−42807.
(16) Beverina, L.; Salice, P. Squaraine Compounds: Tailored Design and Synthesis towards a Variety of Material Science Applications. *Eur. J. Org. Chem.* **2010**, *2010*, 1207−1225.
(17) Wei, G.; Wang, S.; Sun, K.; Thompson, M. E.; Forrest, S. R. Solvent-Annealed Crystalline Squaraine: $PC_{70}BM$ (1:6) Solar Cells. *Adv. Energy Mater.* **2011**, *1*, 184−187.
(18) Wang, S.; Mayo, E. I.; Perez, M. D.; Griffe, L.; Wei, G.; Djurovich, P. I.; Forrest, S. R.; Thompson, M. E. High Efficiency Organic Photovoltaic Cells Based on a Vapor Deposited Squaraine Donor. *Appl. Phys. Lett.* **2009**, *94*, 233304.
(19) Pandey, S. S.; Watanabe, R.; Fujikawa, N.; Ogomi, Y.; Yamaguchi, Y.; Hayase, S. Fine Tuning the Structure of Unsymmetrical Squaraine Dyes Towards the Development of Efficient Dye-Sensitized Solar Cells. *Proc. SPIE* **2011**, *8111*, 811116.
(20) Fabian, J.; Nakazumi, H.; Matsuoka, M. Near-Infrared Absorbing Dyes. *Chem. Rev.* **1992**, *92*, 1197−1226.
(21) So, S.; Choi, H.; Ko, H. M.; Kim, C.; Paek, S.; Cho, N.; Song, K.; Lee, J. K.; Ko, J. Novel Unsymmetrical Push−Pull Squaraine Chromophores for Solution Processed Small Molecule Bulk Heterojunction Solar Cells. *Sol. Energy Mater. Sol. Cells* **2012**, *98*, 224−232.
(22) Yang, D.; Yang, Q.; Yang, L.; Luo, Q.; Huang, Y.; Lu, Z.; Zhao, S. Novel High Performance Asymmetrical Squaraines for Small Molecule Organic Solar Cells with a High Open Circuit Voltage of 1.12 V. *Chem. Commun.* **2013**, *49*, 10465−10467.
(23) Yang, D.; Yang, Q.; Yang, L.; Luo, Q.; Chen, Y.; Zhu, Y.; Huang, Y.; Lu, Z.; Zhao, S. A Low Bandgap Asymmetrical Squaraine for High-Performance Solution-Processed Small Molecule Organic Solar Cells. *Chem. Commun.* **2014**, *50*, 9346−9348.
(24) Yang, L.; Yang, Q.; Yang, D.; Luo, Q.; Zhu, Y.; Huang, Y.; Zhao, S.; Lu, Z. Marked Effects of Indolyl vs. Indolinyl Substituent on Solid-State Structure, Carrier Mobility and Photovoltaic Efficiency of Asymmetrical Squaraine Dyes. *J. Mater. Chem. A* **2014**, *2*, 18313−18321.
(25) Yang, D.; Zhu, Y.; Jiao, Y.; Yang, Q.; Yang, L.; Luo, Q.; Pu, X.; Huang, Y.; Zhao, S.; Lu, Z. *N*,*N*-Diarylamino End-Capping as a New Strategy for Simultaneously Enhancing Open-Circuit Voltage, Short-Circuit Current Density and Fill Factor in Small Molecule Organic Solar Cells. *RSC Adv.* **2015**, *5*, 20724−20733.
(26) Zhou, H.; Yang, L.; Stuart, A. C.; Price, S. C.; Liu, S.; You, W. Development of Fluorinated Benzothiadiazole as a Structural Unit for a Polymer Solar Cell of 7% Efficiency. *Angew. Chem., Int. Ed.* **2011**, *50*, 2995−2998.
(27) Albrecht, S.; Janietz, S.; Schindler, W.; Frisch, J.; Kurpiers, J.; Kniepert, J.; Inal, S.; Pingel, P.; Fostiropoulos, K.; Koch, N.; Neher, D. Fluorinated Copolymer PCPDTBT with Enhanced Open-Circuit Voltage and Reduced Recombination for Highly Efficient Polymer Solar Cells. *J. Am. Chem. Soc.* **2012**, *134*, 14932−14944.
(28) Price, S. C.; Stuart, A. C.; Yang, L.; Zhou, H.; You, W. Fluorine Substituted Conjugated Polymer of Medium Band Gap Yields 7% Efficiency in Polymer−Fullerene Solar Cells. *J. Am. Chem. Soc.* **2011**, *133*, 4625−4631.
(29) Guo, S.; Ning, J.; Korstgens, V.; Yao, Y.; Herzig, E. M.; Roth, S. V.; Muller-Buschbaum, P. The Effect of Fluorination in Manipulating the Nanomorphology in PTB7:$PC_{71}BM$ Bulk Heterojunction Systems. *Adv. Energy Mater.* DOI: 10.1002/aenm.201401315.
(30) Jo, J. W.; Bae, S.; Liu, F.; Russell, T. P.; Jo, W. H. Comparison of Two D−A Type Polymers with Each Being Fluorinated on D and A Unit for High Performance Solar Cells. *Adv. Funct. Mater.* **2015**, *25*, 120−125.
(31) Son, H. J.; Wang, W.; Xu, T.; Liang, Y.; Wu, Y.; Li, G.; Yu, L. Synthesis of Fluorinated Polythienothiophene-*co*-benzodithiophenes and Effect of Fluorination on the Photovoltaic Properties. *J. Am. Chem. Soc.* **2011**, *133*, 1885−1894.
(32) Pan, J.-Y.; Zuo, L.-J.; Hu, X.-L.; Fu, W.-F.; Chen, M.-R.; Fu, L.; Gu, X.; Shi, H.-Q.; Shi, M.-M.; Li, H.-Y.; Chen, H.-Z. Star-Shaped D−A Small Molecules Based on Diketopyrrolopyrrole and Triphenylamine for Efficient Solution-Processed Organic Solar Cells. *ACS Appl. Mater. Interfaces* **2013**, *5*, 972−980.
(33) Zhou, R.; Li, Q.-D.; Li, X.-C.; Lu, S.-M.; Wang, L.-P.; Zhang, C.-H.; Huang, J.; Chen, P.; Li, F.; Zhu, X.-H.; Choy, W. C.H.; Peng, J.; Cao, Y.; Gong, X. A Solution-Processable Diketopyrrolopyrrole Dye Molecule with (Fluoronaphthyl)thienyl Endgroups for Organic Solar Cells. *Dyes Pigm.* **2014**, *101*, 51−57.
(34) Coppo, P.; Plummer, E. A.; Cola, L. D. Tuning Iridium(III) Phenylpyridine Complexes in the "Almost Blue" Region. *Chem. Commun.* **2004**, 1774−1775.
(35) Van der Poll, T. S.; Love, J. A.; Nguyen, T.-Q.; Bazan, G. C. Non-Basic High- Performance Molecules for Solution-Processed Organic Solar Cells. *Adv. Mater.* **2012**, *24*, 3646−3649.
(36) Love, J. A.; Nagao, I.; Huang, Y.; Kuik, M.; Gupta, V. K.; Takacs, C. J.; Coughlin, J. E.; Qi, L.; van der Poll, T. S.; Kramer, E. J.; Heeger, A. J.; Nguyen, T.-Q.; Bazan, G. C. Silaindacenodithiophene-Based Molecular Donor: Morphological Features and Use in the Fabrication of Compositionally Tolerant, High-Efficiency Bulk Heterojunction Solar Cells. *J. Am. Chem. Soc.* **2014**, *136*, 3597−3606.
(37) Moon, M.; Walker, B.; Lee, J.; Park, S. Y.; Ahn, H.; Kim, T.; Lee, T. H.; Heo, J.; Seo, J. H.; Shin, T. J.; Kim, J. Y.; Yang, C. Dithienogermole-Containing Small-Molecule Solar Cells with 7.3% Efficiency: In-Depth Study on the Effects of Heteroatom Substitution of Si with Ge. *Adv. Energy Mater.* DOI: 10.1002/aenm.201402044.

DOI: 10.1021/acsami.5b03558
ACS Appl. Mater. Interfaces 2015, 7, 13675−13684

(38) Scharber, M. C.; Muhlbacher, D.; Koppe, M.; Denk, P.; Waldauf, C.; Heeger, A. J.; Brabec, C. J. Design Rules for Donors in Bulk-Heterojunction Solar Cells—Towards 10% Energy-Conversion Efficiency. *Adv. Mater.* **2006**, *18*, 789−794.
(39) Liess, A.; Huang, L.; Esteban, A. A.; Lv, A.; Gsanger, M.; Stepanenko, V.; Stolte, M.; Wurthner, F. Organic Thin Film Transistors Based on Highly Dipolar Donor−Acceptor Polymethine Dyes. *Adv. Funct. Mater.* **2015**, *25*, 44−57.
(40) Guan, Z.; Yu, J.; Huang, J.; Zhang, L. Power Efficiency Enhancement of Solution-Processed Small-Molecule Solar Cells Based on Squaraine via Thermal Annealing and Solvent Additive Methods. *Sol. Energy Mater. Sol. Cells* **2013**, *109*, 262−269.
(41) Heeger, A. J. 25th Anniversary Article: Bulk Heterojunction Solar Cells: Understanding the Mechanism of Operation. *Adv. Mater.* **2014**, *26*, 10−28.
(42) Mihailetchi, V. D.; Xie, H. X.; de Boer, B.; Koster, L. J. A.; Blom, P. W. M. Charge Transport and Photocurrent Generation in Poly(3-hexylthiophene): Methanofullerene Bulk-Heterojunction Solar Cells. *Adv. Funct. Mater.* **2006**, *16*, 699−708.
(43) Hoppe, H.; Niggemann, M.; Winder, C.; Kraut, J.; Hiesgen, R.; Hinsch, A.; Meissner, D.; Sariciftci, N. S. Nanoscale Morphology of Conjugated Polymer/Fullerene-Based Bulk-Heterojunction Solar Cells. *Adv. Funct. Mater.* **2004**, *14*, 1005−1011.
(44) Chen, G.; Sasabe, H.; Wang, Z.; Wang, X.-F.; Hong, Z.; Yang, Y.; Kido, J. Solution-Processed Organic Photovoltaic Cells Based on a Squaraine Dye. *Phys. Chem. Chem. Phys.* **2012**, *14*, 14661−14666.
(45) Yang, B.; Cox, J.; Yuan, Y.; Guo, F.; Huang, J. Increased Efficiency of Low Band Gap Polymer Solar Cells at Elevated Temperature and its Origins. *Appl. Phys. Lett.* **2011**, *99*, 133302.

DOI: 10.1021/acsami.5b03558
ACS Appl. Mater. Interfaces 2015, 7, 13675−13684